Solar Energy Materials & Solar Cells 230 (2021) 111173

Contents lists available at ScienceDirect

Solar Energy Materials and Solar Cells

journal homepage: www.elsevier.com/locate/solmat

Thermostat property of *Janus* emitter in enclosures

Do Hyeon Kim [a,1], Gil Ju Lee [a,1], Se-Yeon Heo [a], Il-Suk Kang [b,**], Young Min Song [a,*]

[a] School of Electrical Engineering and Computer Science, Gwangju Institute of Science and Technology, Cheomdangwagi-ro 123, Buk-gu, Gwangju, 61005, Republic of Korea

[b] National Nanofab Center, Korea Advanced Institute of Science and Technology, 291 Daehak-ro, Yuseong-gu, Daejeon, 34141, Republic of Korea

ARTICLE INFO

Keywords:
Passive radiative cooling
Space cooling
Janus emitter
Thermostat

ABSTRACT

Passive radiative cooling has been spotlighted as a method to solve environmental problems and fuel depletion. Therefore, various radiative coolers have been studied and applied to lower the surface temperatures of objects such as roof, building exterior, solar cells, and automobiles without any external energy. Furthermore, recently, the research scope of radiative cooling is expanded to enclosed spaces, which is not limited to object cooling. Especially, a *Janus* emitter (JET) which has selective and broadband emission on the separated sides, helps drawing the heat from enclosures efficiently. Using JET enables better cooling of enclosed space in hot weather than conventional emitter, which considers the only emissivity of top side, however, the cooling capability in some cases, that cooling is not required (*i.e.,* night and winter), should be demonstrated for practical applications. This study analyzes the space cooling performance of JET in hot and cool conditions (*e.g.,* day and night). The cooling tendencies with different sizes of enclosed space were also confirmed by heat transfer analysis. Furthermore, systematic experiments with various sized emitters demonstrate the space cooling capability of JET in different conditions (*i.e.,* temperature and volume). These successful demonstrations prove the thermal-managing property of JET regardless of chamber volumes.

1. Introduction

Most cooling technologies consume external energy such as fossil fuels and electrical power. However, a large amount (~20%) of the global energy is used for lowering the temperature by operating cooling systems, which causes the depletion of fossil fuels and environmental issues [1]. To challenge these problems, the development of modern cooling systems for efficient and eco-friendly technologies is becoming an essential topic. For instance, the conventional water cooling systems have been improved by additional nanoparticle and semiconductor to enhance the cooling performance [2–5]. Among the various advanced cooling methods, passive radiative cooling has been spotlighted as alternative cooling technology owing to the characteristic of cooling the objects without any external power (*e.g.,* electricity). High emissivity within the atmospheric transparent window (8–13 μm) enables heat release (~300 K) to outer space (*i.e.,* Universe; 3 K) without any external source and air pollution [6–18]. Thus, the energy-free and environmental sustainable characteristics of radiative cooling allow the wide applications for house roofs [19,20], solar cells [21–23], water cooling [24], colored building exteriors [25,26], dew water harvesting [27,28], textiles [29–31], and wearable devices [32–34].

Recently, the research range of passive radiative cooling has been enlarged to enclosures, not limited to a single object [35,36]. Particularly, a *Janus* emitter (JET) which acts as a selective emitter (SE) on the top side and broadband emitter (BE) on the bottom side, has been reported for efficiently drawing the heat from enclosures [36]. Owing to the dual-emissivity on the separated sides, the bottom side absorbs the inner heat in a broad spectral range (*i.e.,* 4–20 μm), which covers the blackbody radiation at high temperatures (*e.g.,* 333 K). The top side of JET emits the absorbed heat to outer space in the atmospheric window (*i.e.,* 8–13 μm) without absorbing the ambient radiation. Thus, using JET enables the better cooling capability of enclosures in hot weather (*i.e.,* daytime) than conventional radiative cooler (C-RC) which only considers the emissivity of top side such as silicon based micro patterned cooler [37], 2D photonic silica crystal cooler [38], polymer based cooler [39], and PDMS-silica based planar cooler [40]. Although efficient heat dissipation is required in hot enclosures, space cooling is not demanded in cool weather (*i.e,* nighttime). Thus, the cooling capability of JET in

* Corresponding author.
** Corresponding author.
E-mail addresses: iskang@nnfc.re.kr (I.-S. Kang), ymsong@gist.ac.kr (Y.M. Song).
[1] These authors contributed equally to this work.

https://doi.org/10.1016/j.solmat.2021.111173
Received 2 April 2021; Received in revised form 4 May 2021; Accepted 7 May 2021
Available online 19 May 2021

cool enclosures also should be demonstrated for practical applications.

Here, this paper demonstrates the thermal managing characteristic of JET in an enclosed space. The dual-emissivity characteristic is vital for releasing the trapped heat in hot enclosed space (*i.e.*, daytime), while the emissivities at separated sides do not effectively help to lower the temperature of cooled space (*i.e.,* nighttime) compared to C-RC that does not efficiently release the heat in enclosures. The low cooling performance of JET in cold enclosures can be explained by Steffan-Boltzman law which indicates the small thermal radiation caused by similar temperatures between the inner object and outer space [41]. Heat transfer analysis for different temperature conditions (*i.e,* hot and cold) in the enclosure theoretically confirms the thermal property of JET compared with C-RC. The space cooling capability with structure parameters (*i.e.,* height and width of the chamber) was also analyzed to verify the effects of various scaled enclosures. Furthermore, the different sized (*i.e.,* 2-inch and 8-inch) JETs were fabricated, which prove the feasibility of large-area fabrication, and the thermostat property of JET was experimentally demonstrated in both small and large enclosures for 2-inch and 8-inch sized JET. These approaches have significant academic value and application of passive space cooler since the thermostat property of space cooler and scaling effect are less investigated. Thus, the results of this research allow developing the radiative cooling techniques in practical applications.

2. Results and discussion

2.1. Thermal management characteristic of JET

The thermostat characteristic of *Janus* emitter (JET) is presented in Fig. 1a. In the daytime, the temperature of an enclosed car (T_{car}) gets much higher than the ambient temperature (T_{amb}) due to the incident high solar energy and heat trapping in the enclosure, which is called the greenhouse effect. Since the temperature gap between the automobile and ambient air (T_{car} - T_{amb}) gets larger in the day-time, the thermal radiation power exponentially increases according to Stefan-Boltzmann law [41]. In this case, the JET can function as an effective heat channel since the bottom surface absorbs the broadband thermal emission from the hot enclosure (Fig. 1b; bottom). The absorbed heat from the bottom side can be emitted to outer space through the top side of JET due to the selective thermal emission at the top surface. Selective emission in the atmospheric window (*i.e.,* 8–13 μm) at the top side enables efficiently releasing the heat with blocking the atmospheric absorption (Fig. 1b; top). Thus, JET is an effective space cooler in heated enclosures (*e.g.,* daytime) compared with a conventional radiative cooler (C-RC) which considers the only emissivity of the top side for surface cooling.

Moreover, the JET not only presents high efficient cooling when the inner temperature (T_{car}) is higher than ambient temperature (T_{amb}), but also avoids undesired cooling when the temperature gap between inner and outer spaces (T_{car} - T_{amb}) is small, which does not demand cooling (*e.g.,* night-time). Owing to the small temperature difference between the spaces, the radiated thermal energy from the enclosure gets smaller by Stefan-Boltzmann law. Consequently, the broadband thermal absorption at the bottom surface is too small to lower the inner temperature. The emitted heat through the top side of JET is also smaller than that of daytime owing to the small heat absorption from the enclosure, which suppresses unwanted cooling. Therefore, the JET has self-adaptive thermostat property since its heat release capability works when the inner heat is sufficiently trapped. In other words, the JET has an operable thermal threshold.

To achieve both selective and broadband emissions at each separated side, Ag-PDMS groove structure on micro-patterned quartz substrate is used in our designed JET (Fig. 1c). The Ag-PDMS groove causes sSPP resonance, which allows near-ideal selective emission at the top side [36]. The bottom side achieves near-ideal broadband emission due to the thick quartz substrate (500 μm) and PDMS layer (10 μm). The detailed dimension and emissivity spectra of the designed JET are described in Figure S1. Fig. 1d presents the fabricated JET with different sizes of JET (*i.e.*, 2-inch and 8-inch), indicating the feasibility of large-scale fabrication of designed JET.

2.2. Fabrication and characterization of large-scale JET

Fig. 2a exhibits the schematic for the fabrication process of JET. Before patterning process, a quartz substrate was rinsed in acetone, isopropanol alcohol (IPA), and deionized (DI) water by sonication for 5 min to remove undesired residues (Fig. 2a; Step 1). Then, a 70 nm thick Cr layer was deposited on a cleaned quartz substrate by electron beam evaporation (KVE-E2000, Korea Vacuum Tech Ltd., Korea) for the etching mask. A positive photoresist (PR; AZ5214E, MicroChemicals, Germany) was spin-coated at 4000 rpm for 30 s on the quartz substrate with Cr mask. The sample was then baked on a hot plate at 110 °C for 60 s for soft baking. To achieve high resolution in large-scale patterning (*i.e.*, 8-inch), a stepper (i-line stepper, NSR-2205i11D, Nikon Inc., Japan) was used with a patterned mask of JET under an exposure intensity of 11 mW/cm^2 for 5 s (Fig. 2a; Step 2). After the exposure, the UV-exposed sample was developed in a developer (AZ-MIF-300, MicroChemicals, Germany) for 60 s. The sample was then dipped in a Cr wet etchant (CR-7, Transene Company Inc., USA) for patterning of etching mask. After Cr etching, the PR mask was removed using an acetone bath for 5 min (Fig. 2a; Step 3). After that, the reactive ion etching method (Oxford Instruments, UK) was used to anisotropically etch the quartz substrate until a 1.7 μm-thick for 43 min, using CF_4 gas (50 sccm) under a pressure

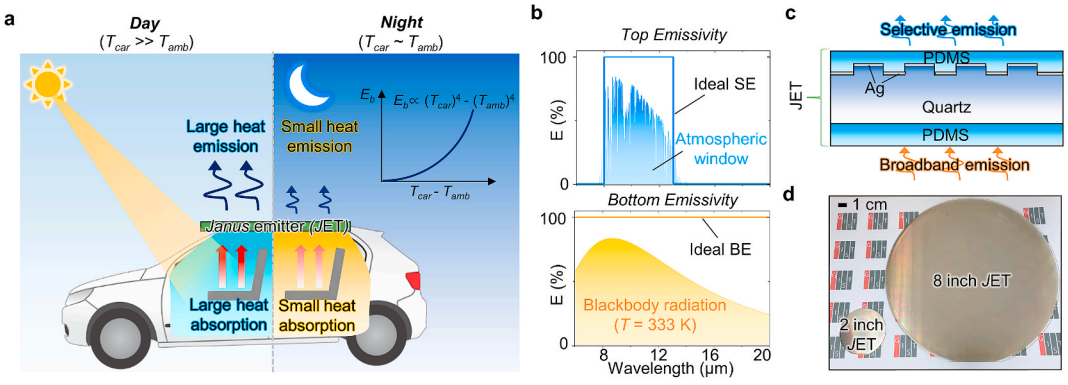

Fig. 1. (a) Schematic of Janus emitter (JET) on an enclosed automobile, where heat is trapped by the greenhouse effect. JET allows large heat emission from space in the daytime while small heat emission in the nighttime. (b) Emissivity spectra of Ideal JET which shows selective emission at the top side, and broadband emission at the bottom side. (c) Cross-sectional schematic of our designed JET, composed of PDMS layers, Ag layer, and micro-patterned quartz. (d) The optical image of fabricated 2-inch and 8-inch sized JET.

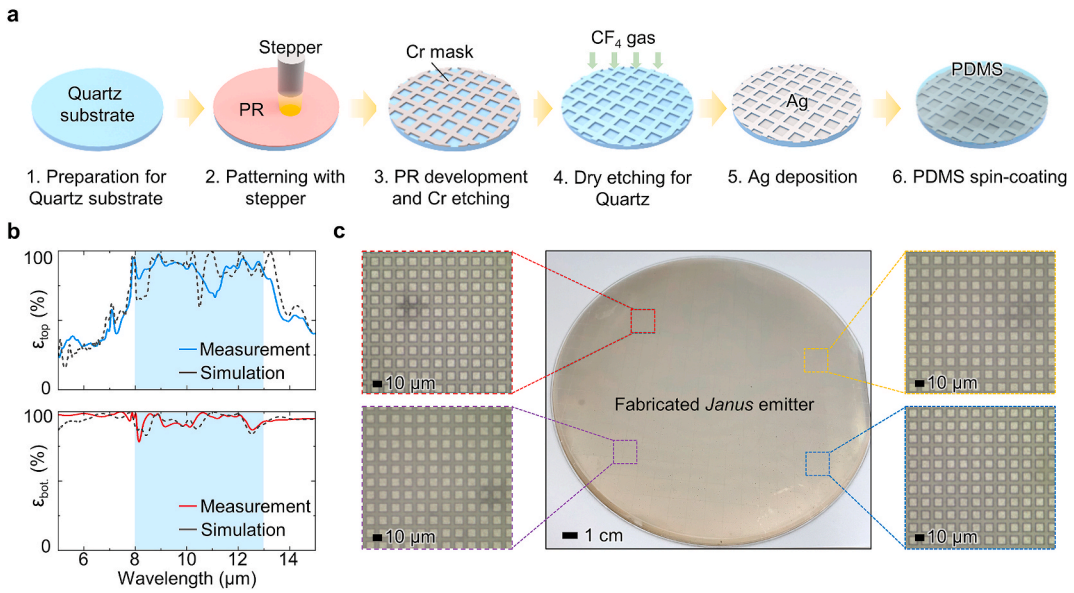

Fig. 2. (a) Fabrication process of JET using MEMS methods for large-area emitter. (b) Measured and simulated emissivity spectra of designed JET at the top side (ε_{top}) and the bottom side ($\varepsilon_{bot.}$) which shows selective and broadband emissions respectively. (c) The optical image of fabricated 8-inch sized JET (middle) with microscopic images at different regions in *Janus* emitter.

of 25 mTorr and an RF power of 60 W. After quartz etching, the Cr mask was removed by immersion in a chrome wet etchant for 30 min (Fig. 2a; Step 4). Then, a 100 nm-thick Ag layer was deposited using an electron beam evaporator at a rate of ~1 Å/s (Fig. 2a; Step 5). After the metal deposition, the PDMS was spin-coated on the Ag-coated quartz groove and bottom side of substrate (Fig. 2a; Step 6).

The measured and simulated emissivity spectra of the designed JET are shown in Fig. 2b. The fabricated JET shows near-ideal selective emission in the atmospheric window region (blue shaded; 8–13 μm) at top side as well as simulated results (Fig. 2b; top). The bottom side of JET also achieves broadband emission in both simulated and measured spectra (Fig. 2b; bottom). Moreover, the optical microscopic images of

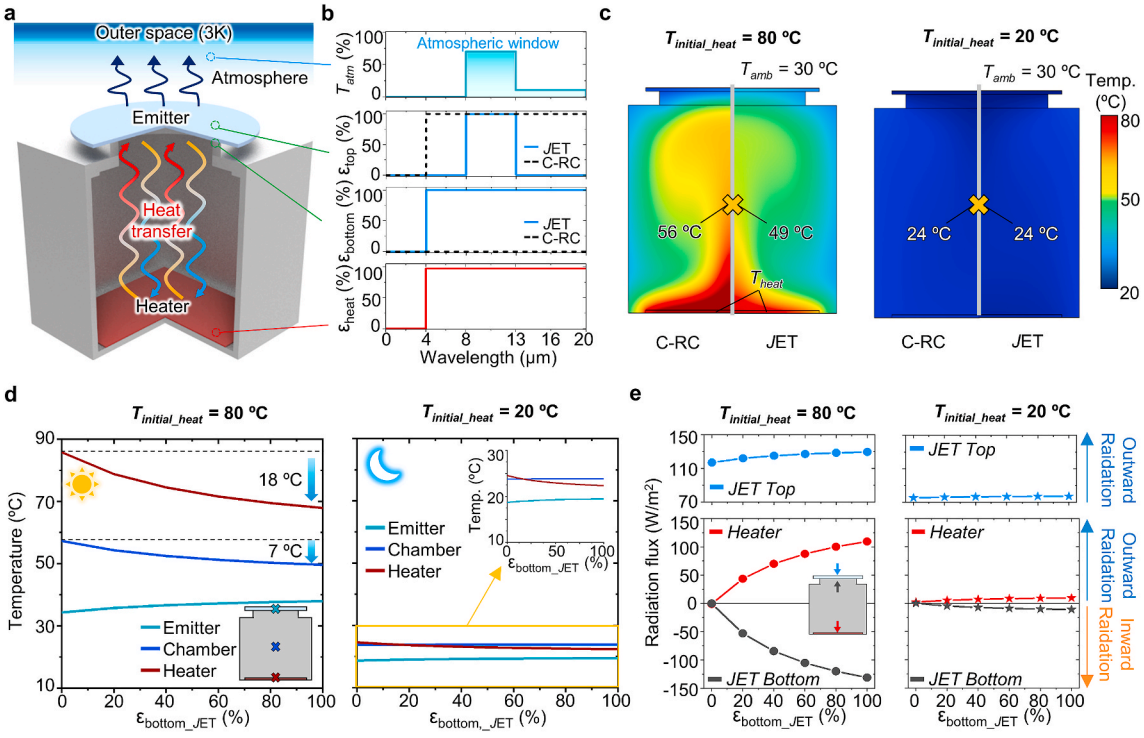

Fig. 3. (a) Schematic illustration of enclosed chamber, used for theoretical heat transfer analysis with conventional radiative cooler (C-RC) and JET. (b) The transmittance of atmospheric window (top), the emissivity spectra of two emitters at the top and bottom sides (middle), and the emissivity of heater which were used in theoretical analysis. (c) Chamber temperature distribution in the case of C-RC and JET with the initial temperatures of heater ($T_{initial\_heat}$) are 80 °C (left) and 20 °C (right) for considering daytime and nighttime respectively. (d) Calculated temperature at the center of emitter, chamber, and heater as a function of JET bottom emissivity (ε_{bottom_JET}) with $T_{initial\_heat}$ = 80 °C (left), and 20 °C (right). (e) Radiation flux at emitter (top and bottom surfaces) and heater (top surface) as a function of ε_{bottom_JET} with different $T_{initial\_heat}$ (*i.e.*, 80 °C (left), and 20 °C (right)).

fabricated 8-inch sized JET at different regions show the same patterns, which proves the uniformity of fabrication (Fig. 2c). The cross-sectional SEM images of fabricated JET also exhibit the desired width and depth as we designed (Figure S2). These results prove the uniform fabrication process of JET on a large-scale.

2.3. Space cooling performances of JET with different enclosure temperatures

To analyze the thermostat property of JET in the enclosed space, the heat transfer analysis method was exploited for simulation using a commercial software (Heat Transfer Module, COMSOL Multiphysics 5.5, USA). The enclosed chamber, which is the domain in the simulation with heat transfer scheme are illustrated in Fig. 3a. The chamber is ideally enclosed space as the emitters cover the top side and heat loss of chamber by ambient air is included for considering practical cases. The condition of non-radiative heat exchange (h_c) between the chamber and ambient air is 3 W/(m^2·K), and the temperature of ambient air (T_{amb}) is 30 °C. The heater which radiates the heat within the enclosure, is placed on the bottom surface for mimicking the heated surface by sunlight through the window of real vehicles. Thus, the initial temperature of heater is set differently (*i.e.,* 80 °C and 20 °C) to consider the hot and cold weather (*i.e.*, day and night). The detailed dimension and initial conditions of simulation domain are described in Figure S3 and Experimental Section/Methods. The emissivity spectra of emitters, heaters and atmospheric transparency, used in calculation, are presented in Fig. 3b. Compared with the JET, C-RC shows broadband emission at top side and zero emissivity at bottom side as it considers surface cooling. The emissivity of heater is as high as (*i.e.,* ~97%) measured emissivity of leather since most interior materials of automobiles consist of leather (Figure S4). Fig. 3c shows the simulated temperature distribution map in hot (*i.e.,* daytime; $T_{initial\_heat}$ = 80 °C) and cool (*i.e.,* night-time; $T_{initial\_heat}$ = 20 °C) enclosures with different coolers (*i.e.,* JET and C-RC) on the top of chambers. In the case of high heater temperature, the JET significantly drops the temperature of entire enclosed space compared with C-RC (Fig. 3c; left). Furthermore, the temperature of chamber center is about 7 °C lower than using C-RC as a space cooler. The temperature of the region which is closed to emitter is slightly higher in JET since the JET absorbs the larger heat from enclosure than C-RC. These results demonstrate that JET has better heat dissipation capability compared with the C-RC in heated enclosed space. In the case of low heater temperature, the temperature distribution of JET is similar to that of C-RC (Fig. 3c; right). Also, the temperatures of chamber center are the same at 24 °C. These results show that JET does not provide undesired cooling in cooled space.

Because the main difference between JET and C-RC is the emissivity of bottom side, the temperatures of main regions in the chamber (*i.e.,* emitter, chamber, and heater) were calculated to verify the cooling performance with different bottom emissivity of JET (Fig. 3d). In the case of $T_{initial\_heat}$ = 80 °C (*i.e.,* daytime), the temperatures of both chamber and heater significantly decrease below 18 °C and 7 °C respectively with increasing bottom emissivity (Fig. 3d; left). On the other hand, the temperature of emitter slightly increases as the larger heat is absorbed by rising emissivity of bottom side. Thus, achieving the high broadband emission of bottom side helps drawing heat away effectively in daytime. Compared with the heated enclosure, the temperature variations (*i.e.,* heater, chamber, and emitter) are very small with growing bottom emissivity in the cooled chamber (Fig. 3; right). The temperature gap of chamber between the emitters of zero and broadband bottom emissivities (*i.e.,* ε_{bottom_JET} = 0% and 100%) is 0.1 °C, which is negligible compared with hot enclosure. The heat transfer process in the enclosure can be confirmed in Fig. 3e. In the hot enclosed space (*i.e.,* daytime; $T_{initial\_heat}$ = 80 °C), the outward radiation flux from heater (red line) increases with the growing bottom emissivity, which indicates that larger heat is emitted from heater (Fig. 3e; left). Thus, the incident radiation flux to bottom of JET (gray line) increases as radiated heat from heater is transferred to the bottom of emitter. By these process, the absorbed heat from bottom side can be dissipated through the top side of emitter. Since the emitter which has high bottom emissivity absorbs the greater amount of heat than the cooler which has low bottom emissivity, the radiated heat from top side gets bigger (blue line). Therefore, the space cooling capability in the heated enclosure is effective with high bottom emissivity. When the enclosure is cooler than previous condition (*i.e.,* night-time; $T_{initial\_heat}$ = 20 °C), the variations of radiation flux are too small to change the temperature of inner space significantly. According to Stefan-Boltzmann law, the radiation power entirely decreases as the temperature gap between the enclosure and ambient air gets reduced. Therefore, the variation of radiation flux with different bottom emissivity is small, which proves the thermostat property of JET.

2.4. Effect of space cooling performance with enclosure dimension

To investigate the effect of space cooling capability with enclosed space dimension (*i.e.,* width and height), the heat analysis with a variation of structure parameters proceeds in Fig. 4a and b. In day-time, the temperature differences of the chamber and the heater between C-RC and JET ($T_{C\text{-}RC}$ - T_{JET}) get larger when the chamber is wider (Fig. 4a; top). As the width of the bottom surface (*i.e.,* heater) increases, the amount of heat radiated from heater gets bigger which grows the internal temperature of the enclosure entirely (Figure S5a and S6a). Similarly, in actual vehicles, car seats proportionally absorb more solar energy to the area of seats. Since JET effectively absorbs the heat from internal space at the bottom surface, the temperature of the region, which is below the emitter, is lower than C-RC (Figure S6a). Due to the larger amount of heat, the temperature gap between the JET and CRC is bigger in a wider chamber. Thus, the $T_{C\text{-}RC}$ - T_{JET} soars with a wider enclosure since the JET releases the heat more efficiently than C-RC in hotter space by Stefan-Boltzmann law. In the night-time, the temperature gap between C-RC and JET is closed to zero regardless of width variation, indicating that JET does not provide unnecessary cooling in contrast with day-time (Fig. 4a; bottom). As the released heat from the heater is small, the width variation does not affect significantly to change the temperatures of the chamber (*i.e.,* emitter, chamber, and heater) (Figure S5a and S6b). Thus, the JET has consistent cooling performance in the night-time regardless of width variation.

When the height of the enclosure increases, the temperature differences of heater and chamber between C-RC and JET decreases in the daytime (Fig. 4b; top). Since the enclosure volume increases with height increment while the width of the heater does not change, the emitted heat per volume decreases which lower the temperature of the enclosed space entirely as shown in Figure S5b and S7a. The smaller amount of heat from the heater can reach the top of the chamber with increasing height (Figure S7a). As the JET absorbs the smaller heat at the bottom surface of the emitter, the cooling capability by bottom emission gets lower with a higher enclosure. Consequently, the temperature gap of chamber and heater between C-RC and JET slightly decrease in a higher enclosure. As the strong heat source does not exist in the nighttime, the temperature differences between C-RC and JET are closed to zero and do not change by height variation (Fig. 4b; bottom). Similar to width variation, the released heat is too small to change the entire temperature of the enclosure (Figure S5b and S7b). Therefore, the JET has a similar cooling capability in the nighttime regardless of height variation. These results show that the difference in cooling temperature may occur depending on the structural parameter change, but the cooling performance trend of C-RC and JET is the same regardless of the structure dimensions.

2.5. Demonstration of cooling capability for JET by temperature measurement

To validate the space cooling capability of JET, the temperature

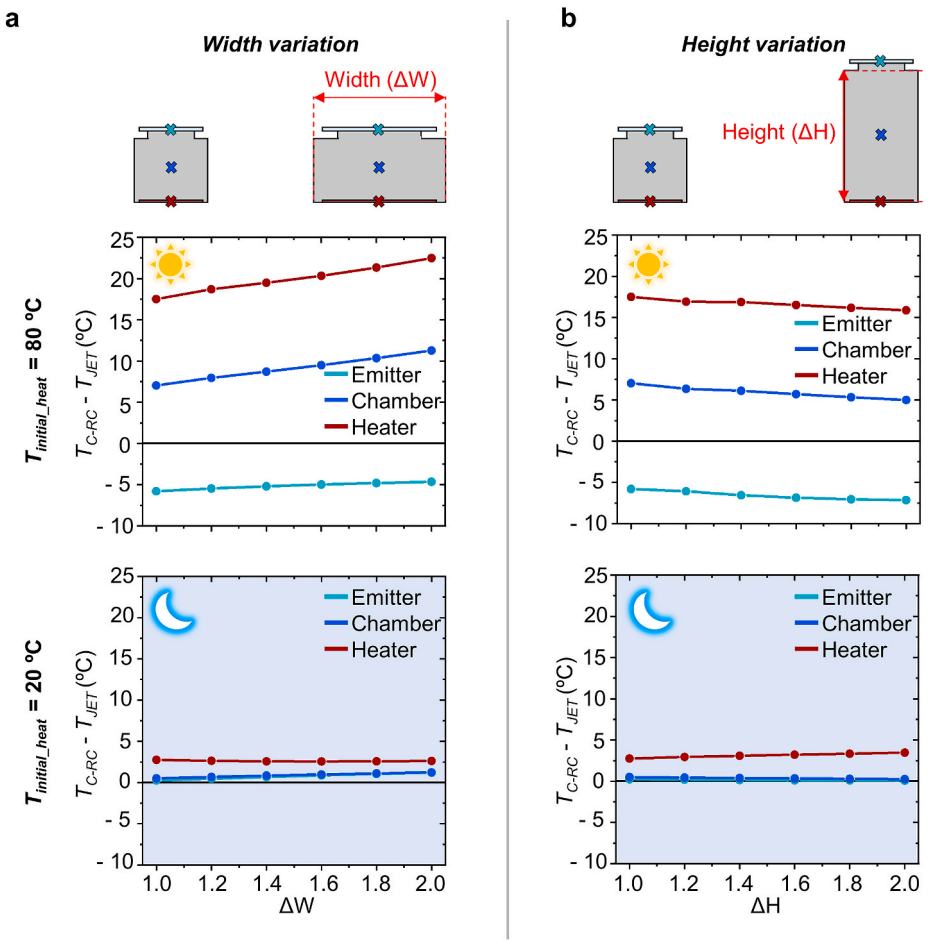

Fig. 4. The calculated temperature difference between the cases using C-RC and *JET* at the center of emitter, chamber, and heater as a function of (a) width and (b) height. The initial value is set to 80 °C (top) and 20 °C (bottom).

recording experiments were conducted using car-shaped chambers with Al metal housing (Fig. 5a). To mimic the stationary vehicle, the solar transparent/IR reflecting window was inserted and black leather was placed on the bottom surface of the chamber, which causes the greenhouse effect (Fig. 5a; top). The temperature sensor was attached below the radiative object (leather) and the emitter was placed on top of the chamber. To confirm the effect of chamber dimension, the different sizes of chambers, applicable for 2 and 8-inch sized emitters were used for experiments (Fig. 5a; bottom). The C-RC is fabricated by acrylic coating on Al substrate and the emissivity shows the broadband in the IR region (Figure S8).

The outdoor experimental measurement results are presented in Fig. 5b. In the daytime, the incident sunlight through the window heats the radiative object and the heated object radiates the heat in the enclosure, which causes the greenhouse effect. As the temperature of the chamber entirely rises by the greenhouse effect, the *JET* achieves 4.9

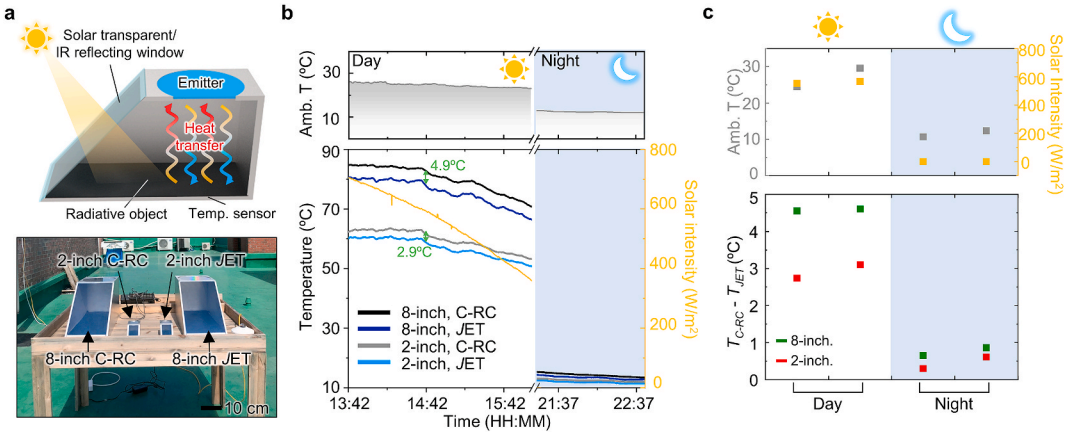

Fig. 5. (a) Schematic illustration (top) and photograph of measurement setup, designed in the shape of an automobile. (b) Temperature measurement of radiative object for different emitters (*i.e.*, C-RC and *JET*) with 8-inch and 2-inch size. (c) Measurements for two days and nights with different weather conditions of solar intensity and ambient temperature.

and 2.9 °C lower than C-RC in 8-inch and 2-inch groups respectively in the heated chamber. The reason for the cooling temperature difference between 8-inch and 2-inch groups is due to the larger Al wall absorbs more heat than small chambers. Thus, the bigger chambers containing 8-inch emitters get more heat than smaller chambers, which causes a larger temperature difference between C-RC and *J*ET. On the other hand, *J*ET achieves 0.7 and 0.6 °C than C-RC in 8-inch and 2-inch groups respectively in the nighttime which means a similar cooling performance. As there is no strong heat source (*i.e.,* sunlight) to heat the chamber, the temperature difference is much smaller than daytime.

Repeated measurements for two different days and nights demonstrate the thermal managing property of *J*ET (Fig. 5c). The detailed raw data is shown in Figure S9. *J*ET has better space cooling capability than C-RC in several daytimes which have average solar powers of ~600 W/m^2. And *J*ET has a similar cooling performance with C-RC in two nights. Therefore, *J*ET shows better cooling capability in the daytime and does not provide undesired cooling in the night-time regardless of chamber size, which proves the thermostat characteristic of *J*ET.

3. Conclusion

In this study, the thermostat property of *J*ET in enclosed space was demonstrated in the case of hot and cold days by heat transfer calculation and outdoor experiments. As the bidirectional emission characteristics help drawing the trapped heat to outer space, *J*ET lowers the temperature of hot enclosures than that of C-RC about 5 °C at maximally in the daytime. On the other hand, *J*ET lowers the temperature of cold space than C-RC about <0.5 °C on average in the nighttime, which is a negligible difference compared with daytime. These experimental results indicate that *J*ET does not provide undesired cooling in the cold enclosure when the cooling is avoided as the enclosure temperature is similar to outer ambient temperature (*i.e.*, night-time). The cooling capability with the variation of structure parameters (*i.e.,* width and height of the enclosure) was also investigated. The cooling temperature of emitters can slightly vary by width and height variation, however, the thermostat characteristic of *J*ET is still applicable regardless of the shape of the chambers. These results indicate the versatility of *J*ET in various weather conditions which can be adapted to various applications such as stationary automobiles.

4. Experimental Section/Methods

Optical simulation: To simulate the emissivity spectra of several structures, rigorous coupled wave analysis-based commercial software (DiffractMOD, RSoft Design Group, Synopsys, USA) was employed. Absorption profiles were also simulated using this software. In all the simulations, a 0.5 nm-square grid size was utilized to numerically calculate the stable emissivity.

Characterization: The emissivity spectra were characterized by measuring the reflectance spectra of the samples using a Fourier transform infrared spectrometer (Spectrum Paragon, PerkinElmer, Inc., USA) with an Au-coated integrating sphere to detect the diffuse reflection. Because the infrared rays cannot pass through even a thin Al layer, the emissivity spectra were derived from the measured reflectance spectra (*i.e.,* E = 1 - R). SEM (S-4700, Hitachi Hi-Technologies, Japan) was utilized to observe the cross-section of the fabricated *J*ET.

Heat transfer simulation: 2D steady-state thermal energy equation was used for the enclosure with the natural convection inside the enclosure due to the buoyancy-driven flow by the heater. The heat conduction through the solid region was implemented by forcing the local velocity to zero. Furthermore, the surface to surface radiation exchange based on view factor was also included in the model. For the inner surface, only the heater was assumed to be perfectly thermal insulated.

Credit author statement

Do Hyeon Kim: Conceptualization, Methodology, Investigation, Resources, Software, Validation, Formal analysis, Data Curation, Writing - Original Draft, Writing - Review & Editing, Visualization.

Gil Ju Lee: Conceptualization, Methodology, Investigation, Formal analysis, Resources, Data curation, Writing- Original draft, Writing - Review & Editing.

Se-Yeon Heo: Conceptualization, Software, Resources.

Il-Suk Kang: Resources.

Young Min Song: Supervision.

Declaration of competing interest

The authors declare that they have no known competing financial interests or personal relationships that could have appeared to influence the work reported in this paper.

Acknowledgements

This work was supported by the National Research Foundation of Korea (NRF-2020R1A2C2004983/2018M3D1A1058997/NRF2018R1A4A1025623) and by the GIST Research Institute (GRI) grant funded by the GIST in 2021. G. J. Lee was supported by the National Research Foundation of Korea (NRF- 2021R1C1C2013605).

Appendix A. Supplementary data

Supplementary data to this article can be found online at https://doi.org/10.1016/j.solmat.2021.111173.

References

[1] IEA, The Future of Cooling. www.iea.org/reports/the-future-of-cooling. (Accessed May 2018).
[2] C. Qi, T. Chen, J. Tu, Y. Wang, Kor. J. Chem. Eng. 37 (2020) 2104.
[3] T. Chen, C. Qi, J. Tang, G. Wang, Y. Yan, Case Stud. Therm. Eng. 24 (2021) 100848.
[4] M.H. Esfe, M. Afrand, Physica A 540 (2020) 120766.
[5] Y. Hu, Y. He, C. Qi, B. Jiang, H.I. Schlaberg, Int. J. Heat Mass Tran. 78 (2014) 380.
[6] L. Zhu, A. Raman, S. Fan, Appl. Phys. Lett. 103 (2013) 223902.
[7] M. Kim, J. Seo, S. Yoon, H. Lee, J. Lee, B.J. Lee, J. Quant. Spectrosc. Radiat. Transf. 260 (2021) 107475.
[8] A. Leroy, B. Bhatia, C.C. Kelsall, A. Castillejo-Cuberos, M.D. Capua, L. Zhao, L. Zhang, A.M. Guzman, E.N. Wang, Sci. Adv. 5 (2019) eaat9480.
[9] S. Jeon, S. Son, S.Y. Lee, D. Chae, J.H. Bae, H. Lee, S.J. Oh, ACS Appl. Mater. 12 (2020) 54763.
[10] A.P. Raman, M.A. Anoma, L. Zhu, E. Rephaeli, S. Fan, Nature 515 (2014) 540.
[11] S. Atiganyanun, J.B. Plumley, S.J. Han, K. Hsu, J. Cytrynbaum, T.L. Peng, S. M. Han, S.E. Han, ACS Photonics 5 (2018) 1181.
[12] L. Fan, W. Li, W. Jin, M. Orenstein, S. Fan, Opt Express 28 (2020) 25460.
[13] S. Jeon, J. Shin, Sci. Rep. 10 (2020) 1.
[14] J. Jaramillo-Fernandez, G.L. Whitworth, J.A. Pariente, A. Blanco, P.D. Garcia, C. Lopez, C.M. Sotomayor-Torres, Small 15 (2019) 1905290.
[15] J. Mandal, Y. Fu, A.C. Overvig, M. Jia, K. Sun, N.N. Shi, H. Zhou, X. Xiao, N. Yu, Y. Yang, Science 362 (2018) 315.
[16] J. Song, J. Seo, J. Han, J. Lee, B.J. Lee, Appl. Phys. Lett. 117 (2020), 094101.
[17] D. Chae, M. Kim, P.H. Jung, S. Son, J. Seo, Y. Liu, B.J. Lee, H. Lee, ACS Appl. Mater. Interfaces 12 (2020) 8073.
[18] S. Jeon, J. Shin, Opt Express 29 (2021) 8376.
[19] J. Chen, L. Lu, J. Build. Eng. 33 (2021) 101631.
[20] W. Wang, N. Fernandez, S. Katipamula, K. Alvine, Renew. Energy 118 (2018) 265.
[21] L. Zhu, A. Raman, K.X. Wang, M.A. Anoma, S. Fan, Optica 1 (2014) 32.
[22] B. Zhao, M. Hu, X. Ao, G. Pei, Sol. Energy 176 (2018) 248.
[23] Z. Chen, L. Zhu, W. Li, S. Fan, Joule 3 (2019) 101.
[24] D. Zhao, A. Aili, Y. Zhai, J. Lu, D. Kidd, G. Tan, X. Yin, R. Yang, Joule 3 (2019) 111.
[25] T. Li, Y. Zhai, S. He, W. Gan, Z. Wei, M. Heidarinejad, D. Dalgo, R. Mi, X. Zhao, J. Song, J. Dai, C. Chen, A. Aili, A. Vellore, A. Martini, R. Yang, J. Srebric, X. Yin, L. Hu, Science 364 (2019) 760.
[26] G.J. Lee, Y.J. Kim, H.M. Kim, Y.J. Yoo, Y.M. Song, Adv. Opt. Mater. 6 (2018) 1800707.
[27] D. Beysens, M. Muselli, I. Milimouk, C. Ohayon, S.M. Berkowicz, E. Soyeux, M. Mileta, P. Ortega, Energy 31 (2006) 2303.
[28] D. Zhao, A. Aili, Y. Zhai, S. Xu, G. Tan, X. Yin, R. Yang, Appl. Phys. Rev. 6 (2019), 021306.

[29] P.-C. Hsu, X. Liu, C. Liu, X. Xie, H.R. Lee, A.J. Welch, T. Zhao, Y. Cui, Nano Lett. 15 (2015) 365.
[30] P.-C. Hsu, A.Y. Song, P.B. Catrysse, C. Liu, Y. Peng, J. Xie, S. Fan, Y. Cui, Science 353 (2016) 1019.
[31] Y. Peng, J. Chen, A.Y. Song, P.B. Catrysse, P.-C. Hsu, L. Cai, B. Liu, Y. Zhu, G. Zhou, D.S. Wu, H.R. Lee, S. Fan, Y. Cui, Nat. Sustain. 1 (2018) 105.
[32] M.H. Kang, G.J. Lee, J.H. Lee, M.S. Kim, Z. Yan, J.W. Jeong, Y.M. Song, Adv. Sci. (2021) 2004885.
[33] Y. Xu, B. Sun, Y. Ling, Q. Fei, Z. Chen, X. Li, P. Guo, N. Jeon, S. Goswami, Y. Liao, S. Ding, Q. Yu, J. Lin, G. Huang, Z. Yan, Proc. Natl. Acad. Sci. Unit. States Am. 117 (2020) 205.
[34] H. Zhang, K.C.S. Ly, X. Liu, Z. Chen, M. Yan, Z. Wu, X. Wang, Y. Zheng, H. Zhou, T. Fan, Proc. Natl. Acad. Sci. Unit. States Am. 117 (2020) 14657.
[35] S.Y. Jeong, C.Y. Tso, M. Zouagui, Y.M. Wong, C.Y. Chao, Build. Simul. 11 (2018) 1011.
[36] S.-Y. Heo, G.J. Lee, D.H. Kim, Y.J. Kim, S. Ishii, M.S. Kim, T.J. Seok, B.J. Lee, H. Lee, Y.M. Song, Sci. Adv. 6 (2020) eabb1906.
[37] G.J. Lee, D.H. Kim, S.-Y. Heo, Y.M. Song, ACS Appl. Mater. Interfaces 12 (2020) 53206.
[38] X. Sun, Y. Sun, Z. Zhou, M.A. Alam, P. Bermel, Nanophotonics 6 (2017) 997.
[39] J. Mandal, Y. Yang, N. Yu, A.P. Raman, Joule 4 (2020) 1350.
[40] J.-L. Kou, Z. Jurado, Z. Chen, S. Fan, A.J. Minnich, ACS Photonics 4 (2017) 626.
[41] P.A. Constantinides, Am. J. Phys. 9 (1941) 87.